Sequence intrinsic somatic mutation mechanisms contribute to affinity maturation of VRC01-class HIV-1 broadly neutralizing antibodies

Joyce K. Hwang[a,b,c,d], Chong Wang[a,b,c,d], Zhou Du[a,b,c,d], Robin M. Meyers[a,b,c,d], Thomas B. Kepler[e], Donna Neuberg[f], Peter D. Kwong[g], John R. Mascola[g], M. Gordon Joyce[g], Mattia Bonsignori[h], Barton F. Haynes[h], Leng-Siew Yeap[a,b,c,d,1,2], and Frederick W. Alt[a,b,c,d,2,3]

[a]Howard Hughes Medical Institute, Boston Children's Hospital, Boston, MA 02115; [b]Program in Cellular and Molecular Medicine, Boston Children's Hospital, Boston, MA 02115; [c]Department of Pediatrics, Harvard Medical School, Boston, MA 02115; [d]Department of Genetics, Harvard Medical School, Boston, MA 02115; [e]Department of Microbiology, Boston University School of Medicine, Boston, MA 02215; [f]Department of Biostatistics and Computational Biology, Dana-Farber Cancer Institute, Boston, MA 02215; [g]Vaccine Research Center, National Institute of Allergy and Infectious Diseases, National Institutes of Health, Bethesda, MD 20892; and [h]Duke Human Vaccine Institute, Department of Medicine, Duke University School of Medicine, Duke University Medical Center, Durham, NC 27710

Contributed by Frederick W. Alt, June 26, 2017 (sent for review June 5, 2017; reviewed by Jayanta Chaudhuri and Cornelis Murre)

Variable regions of Ig chains provide the antigen recognition portion of B-cell receptors and derivative antibodies. Ig heavy-chain variable region exons are assembled developmentally from V, D, J gene segments. Each variable region contains three antigen-contacting complementarity-determining regions (CDRs), with CDR1 and CDR2 encoded by the V segment and CDR3 encoded by the V(D)J junction region. Antigen-stimulated germinal center (GC) B cells undergo somatic hypermutation (SHM) of V(D)J exons followed by selection for SHMs that increase antigen-binding affinity. Some HIV-1–infected human subjects develop broadly neutralizing antibodies (bnAbs), such as the potent VRC01-class bnAbs, that neutralize diverse HIV-1 strains. Mature VRC01-class bnAbs, including VRC-PG04, accumulate very high SHM levels, a property that hinders development of vaccine strategies to elicit them. Because many VRC01-class bnAb SHMs are not required for broad neutralization, high overall SHM may be required to achieve certain functional SHMs. To elucidate such requirements, we used a V(D)J passenger allele system to assay, in mouse GC B cells, sequence-intrinsic SHM-targeting rates of nucleotides across substrates representing maturation stages of human VRC-PG04. We identify rate-limiting SHM positions for VRC-PG04 maturation, as well as SHM hotspots and intrinsically frequent deletions associated with SHM. We find that mature VRC-PG04 has low SHM capability due to hotspot saturation but also demonstrate that generation of new SHM hotspots and saturation of existing hotspot regions (e.g., CDR3) does not majorly influence intrinsic SHM in unmutated portions of VRC-PG04 progenitor sequences. We discuss implications of our findings for bnAb affinity maturation mechanisms.

broadly neutralizing antibodies | HIV-1 | somatic hypermutation | intrinsic mutability | activation-induced cytidine deaminase

Antibodies are the secreted form of B-cell antigen receptors (BCRs) and are composed of Ig chains. Exons that encode antigen-binding variable regions ("V(D)J exons") of Ig heavy (IgH) chains are assembled in developing B lymphocytes from V (V_H), D, and J (J_H) gene segments by V(D)J recombination. Two antigen-contacting complementarity determining regions (CDRs) are encoded in the germline V_H, whereas CDR3 is created somatically via V(D)J junctional assembly (1). Within the $V_H(D)J_H$ exon, CDRs are embedded within framework regions (FWRs) that are relatively invariant in sequence because they encode requisite variable region structural features (2). About two-thirds of IgH V(D)J rearrangements occur in a "nonproductive" translational reading frame and do not produce functional IgH proteins. B cells often have a nonproductive IgH V(D)J exon in addition to the productive IgH allele that supports B-cell development (3). In response to antigen activation, mature B lymphocytes in germinal centers (GCs) of peripheral lymphoid organs undergo somatic hypermutation (SHM) of Ig V(D)J exons. Cycles of SHM and selection of clones with SHMs that increase BCR-antigen affinity lead to antibody affinity maturation (4). SHM is initiated by activation-induced cytidine deaminase (AID), which deaminates cytosines to uracils that are processed to generate mutations (5). SHM occurs on both DNA strands of productive and nonproductive alleles (5, 6). Transcription is required for SHM of V(D)J exons (5).

Within V(D)J exons predominant AID-targeting sites are at cytidines of short DGYW motifs (D = A/G/T, Y = C/T, W = A/T), with the palindromic AGCT motif representing a canonical example (7). However, whereas DGYW motifs in CDRs often are highly targeted, the same motifs in adjacent FWRs often are not (6, 8). The basis for differential AID targeting of identical hotspot motifs within a transcribed V(D)J exon is unknown. SHM of certain V(D)J hotspots has been proposed to influence subsequent

Significance

B lymphocytes produce antibodies that provide protection from infections. Such antibodies evolve from precursors via pathogen-driven affinity maturation. Affinity maturation involves introduction of somatic hypermutations (SHMs) into antibody genes followed by selection of B lymphocytes producing antibodies that better neutralize the pathogen. Some HIV-1–infected humans develop broadly neutralizing antibodies (bnAbs) that recognize diverse HIV-1 strains. VRC01 is a potent bnAb that binds a crucial portion of HIV-1. Development of vaccine strategies to elicit VRC01-class antibodies is difficult due to the high SHM levels associated with their maturation. We report contributions of sequence-intrinsic mechanisms to the SHM patterns of a VRC01-class bnAb and its precursors in mice. Our findings provide insights into roles of antibody gene sequences in guiding bnAb maturation.

Author contributions: J.K.H., L.-S.Y., and F.W.A. designed research; J.K.H., C.W., and L.-S.Y. performed research; R.M.M., P.D.K., J.R.M., M.G.J., M.B., and B.F.H. contributed new reagents/analytic tools; J.K.H., C.W., Z.D., T.B.K., D.N., L.-S.Y., and F.W.A. analyzed data; and J.K.H. and F.W.A. wrote the paper.

Reviewers: J.C., Memorial Sloan Kettering Cancer Center; and C.M., University of California, San Diego.

The authors declare no conflict of interest.

Data deposition: The sequence reported in this paper has been deposited in the National Center for Biotechnology Information Sequence Read Archive (accession no. SRP111486).

[1]Present address: Shanghai Institute of Immunology, Department of Immunology and Microbiology, The Ministry of Education Key Laboratory of Cell Death and Differentiation, Shanghai Jiao Tong University School of Medicine, Shanghai 200025, China.

[2]L.-S.Y. and F.W.A. share senior authorship.

[3]To whom correspondence should be addressed. Email: alt@enders.tch.harvard.edu.

This article contains supporting information online at www.pnas.org/lookup/suppl/doi:10.1073/pnas.1709203114/-/DCSupplemental.

AID targeting of others within the same sequence (9–11). However, experimental testing of this notion led to divergent conclusions, with transgene studies suggesting that V exon SHM hotspot targeting suppresses that of other hotspots (9) and cell line studies suggesting that hotspot targeting activates additional SHM hotspots (10, 11). Further clarification of the influence of specific SHMs, or SHMs in general, on subsequent targeting of other V exon sequences is important for elucidating mechanisms by which particular V(D)J sequences might influence the course of antibody affinity maturation.

Broadly neutralizing antibodies (bnAbs) against HIV-1 arise in a subset of HIV-1–infected patients (12). VRC01-class bnAbs bind the highly conserved CD4 binding site of HIV envelope gp120 as a structural mimic of CD4 and are among the most potent HIV-1 bnAbs (13). All VRC01-class bnAbs use the human V_H1-2*02 segment (or the highly homologous V_H1-46*01) and contain very high numbers of SHMs (up to 32% of V_HDJ_H exon nucleotides) (13, 14). During the development of HIV-1 bnAbs in an infected individual, SHMs of unmutated germline precursor V_H exon accumulate in affinity maturation intermediates that can be connected to the fully mutated mature antibody (12). Many SHMs in V_H1-2*02–using bnAb sequences occur in V_H1-2*02–using V(D)J exons of non-HIV-1–infected patients, suggesting they result from targeting of sequences intrinsically prone to SHM (15). However, critical SHMs also may occur in V_H1-2*02–using V(D)J exons at sequences with intrinsically low SHM, requiring high overall SHM levels to achieve them. In support of this notion, only a fraction of mature VRC01-class bnAb SHMs are required for broad neutralizing activity (16–18).

We recently developed a mouse V(D)J exon passenger allele system to assay patterns and levels of intrinsic SHMs of desired test sequences in GC B cells (6). We now use this approach to assay intrinsic SHM across passenger substrates that represent various stages in the maturation of a human VRC01-class bnAb lineage. We identify potentially rate-limiting SHMs and reveal how SHM-targeting frequencies change during this VRC01-class bnAb maturation process.

Results

Overview of V(D)J Passenger Allele System. Our passenger allele approach assays GC B-cell SHM-targeting frequencies of test sequences inserted into the passenger IgH V(D)J allele of a "VB1-8/passenger allele" ES cell line (6) (Fig. S1 *A* and *B*). The "productive" allele in this line encodes a B1-8 antibody IgH V(D)J ("VB1-8") exon that supports B-cell development, whereas the passenger harbors a desired test sequence that cannot encode a protein and thus provides intrinsic SHM patterns (6). ES cell lines containing given passenger sequences are used for RAG-2–deficient blastocyst complementation (19) to generate chimeric mice in which all peripheral B cells derive from the modified passenger ES cell (6). Our current studies of V_H1-2*02–related passenger alleles is facilitated by assaying Peyer's patches (PP) GC B-cell intrinsic SHM patterns, because PP GC B-cell VB1-8 productive and passenger sequences have the same general patterns and levels of intrinsic SHM whether or not mice are immunized (6). To visualize hotspot emergence and study accumulation of SHMs on productive and passenger sequences we compare the SHM pattern of sequences in low (3–10 mutations per sequence), intermediate (11–20), and high (21–30) mutational strata, which allows a "pseudo-kinetic" analysis of the appearance of individual SHMs (6). This stratification enables identification of "primary" and "secondary" hotspots, respectively, as those that first appear in the low SHM strata and those that first appear in intermediate SHM strata (Fig. 1; discussed below). In the highest SHM strata, primary hotspots become saturated and SHMs accumulate in nonhotspot regions (6).

CDR3 SHM Does Not Influence Intrinsic SHM Targeting of the Adjacent V_H1-2*02 Segment. To test the notion that SHMs of AID targets in a sequence may influence subsequent SHM of other targets (9–11)

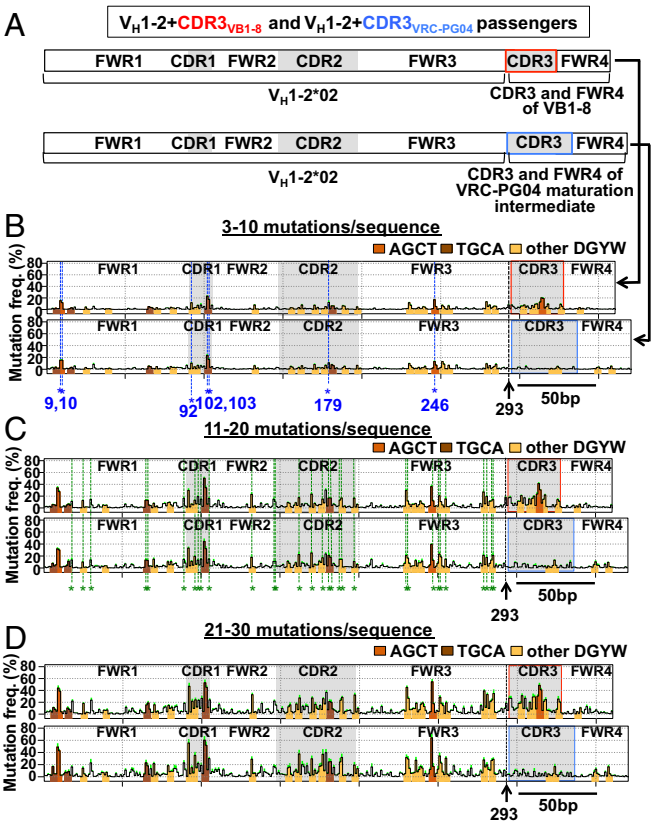

Fig. 1. SHM targeting of V_H1-2*02 attached to CDR3s with different SHM potentials. (*A*) Schematic of V_H1-2*02+CDR3$_{VB1-8}$ and V_H1-2*02+CDR3$_{VRC-PG04}$ passenger test sequences. The V_H1-2*02+CDR3$_{VB1-8}$ passenger (*Top*) is the V_H1-2*02 sequence attached to VB1-8 CDR3 (red box) and VB1-8 FWR4 sequences, followed by VB1-8 J_H2 intron sequence. The V_H1-2*02+CDR3$_{VRC-PG04}$ passenger (*Bottom*) is composed of V_H1-2*02 attached to CDR3 (blue box) and FWR4 of a hypermutated VRC-PG04 maturation intermediate (int16.5% in Fig. S5*A*). (*B–D*) Map of mutations (SHM profile) on V_H1-2*02+CDR3$_{VB1-8}$ (*Top*) and V_H1-2*02+CDR3$_{VRC-PG04}$ (*Bottom*) passenger sequences. *y* axis indicates mutation frequency plotted as the mean percent of sequences mutated at the indicated nucleotide ± SEM (green shading indicates top error bar). n = 9 V_H1-2*02+CDR3$_{VB1-8}$ chimeras and 8 V_H1-2*02+CDR3$_{VRC-PG04}$ chimeras, 3,000–5,000 mutated sequences per chimera. SHM profiles are shown separately for reads with (*B*) 3–10, (*C*) 11–20, or (*D*) 21–30 mutations within the V_H. Blue and green asterisks/dotted lines indicate primary and secondary hotspot positions, respectively. Secondary hotspot positions are listed in Table S1.

we assayed intrinsic SHM levels of the human V_H1-2*02 germline passenger sequence attached to either the VB1-8 CDR3 that has not been subjected to SHM (6, 20) or to the CDR3 of an affinity maturation intermediate of VRC01-class bnAb VRC-PG04 that has undergone extensive SHM (21) (termed V_H1-2+CDR3$_{VB1-8}$ and V_H1-2*02+CDR3$_{VRC-PG04}$, respectively, Fig. 1*A*). In this regard, we hypothesized that the latter CDR3 may have saturated intrinsic hotspots and lack robust SHM targeting activity. We assayed nine VB1-8/V_H1-2*02+CDR3$_{VB1-8}$ and eight VB1-8/V_H1-2*02+CDR3$_{VRC-PG04}$ passenger chimeras. In these experiments, the VB1-8 productive alleles all had similar overall mutation levels and patterns (Figs. S1*C* and S2 *A–C*), indicating that the two distinct passenger sequences were subjected to comparable levels of AID activity and validating their direct comparison. In the low mutation stratum, seven V_H1-2*02 primary hotspot positions were reproducibly mutated in >10% of sequences in both V_H1-2*02+CDR3$_{VB1-8}$ and V_H1-2*02+ CDR3$_{VRC-PG04}$ passengers (Fig. 1*B*, blue asterisks). These primary V_H1-2*02 SHM hotspots include the G and C (positions 9 and 10) of AGCT in FWR1, the G (position 92) of GGCT in CDR1, the G and C

(positions 102 and 103) of TGCA in CDR1, an A (position 179) in CDR2, and the G (position 246) of the AGCT in FWR3. We note that some of these primary hotspots are not predicted from computational models that defined the DGYW motif (7) or enrichment of targeting to CDRs (8), because they either are not at a DGYW motif or they occur in FWRs. At the intermediate mutational stratum, 31 additional secondary hotspot positions are reproducibly mutated in >10% of sequences of both passengers (Fig. 1*C*, green asterisks). At the highest mutational stratum (21–30 mutations per sequence), primary and secondary hotspot positions are still dominant in the SHM landscape, but SHMs of many other positions reproducibly rise above background (Fig. 1*D*). We conclude that individual V_H1-2*02 nucleotides vary widely in intrinsic mutation frequency.

The CDR3 portion of the V_H1-2+$CDR3_{VB1-8}$ passenger was highly targeted for SHM, whereas the CDR3 portion of the V_H1-2*02+ $CDR3_{VRC-PG04}$ passenger was not (Fig. 1 *B–D* and Fig. S1*D*). However, overall mutation frequencies of the V_H1-2*02 segments in these two passengers were not significantly different, whether calculated over the entire V_H (Fig. S1*C*) or over each CDR1, CDR2, or FWR region separately (Fig. S1*D*). We further compared SHM frequencies of the two passengers at each of the 294 nucleotide positions of the V_H1-2*02 sequence and at each stratum (*Materials and Methods*). The only significant difference detected was at position 293, 2 bp upstream of CDR3, which was more highly targeted in V_H1-2*02+$CDR3_{VB1-8}$ versus V_H1-2*02+$CDR3_{VRC-PG04}$ (Fig. 1 *B–D*, arrow and Fig. S1*E*). However, no significant difference in SHM frequency was detected at position 246, which is the primary SHM hotspot (the G of the AGCT of FWR3) most proximal to CDR3 (Fig. S1*F*). These findings suggest that overall SHM of a rearranged V_H1-2*02 segment occurs largely independently of the SHM status of the CDR3 to which it is fused. To further test independence of V_H1-2*02 SHM from that of its associated CDR3 we examined SHM patterns of nonproductively rearranged, and therefore not selected, V_H1-2*02-DJ exon sequences generated endogenously via V(D)J recombination in a V_H1-2*02–rearranging mouse model that generates extremely diverse CDR3s (22). Even in the context of diverse CDR3s the SHM pattern of nonproductively rearranged V_H1-2*02-DJ exon sequences was highly similar to that of the V_H1-2*02 passenger at each tested SHM stratum (Pearson's r = 0.87–0.90) (Fig. S3). The only exceptions were position 10, which is a primary hotspot in the V_H1-2*02 passenger and a secondary hotspot in nonproductive V_H1-2*02-DJ exon sequences, and positions 18 and 30, which are secondary hotspots in the V_H1-2*02 passengers and not hotspots in nonproductively rearranged V_H1-2*02 sequences (Fig. S3). Slightly increased SHM of promoter-proximal V_H1-2*02 sequences in passenger sequence versus endogenously assembled V(D)J exons in V_H1-2*02–rearranging mice may reflect the V_H1-2*02 passenger's being 33 bp more distal to the promoter than the endogenously assembled V(D)J exon, given that SHM is potentially diminished in the promoter-proximal region of transgenic V exons (23).

Similar to what we previously described for the passenger mouse VB1-8 sequence (6), the human V_H1-2*02 passengers had frequent deletions (Fig. 2 *A* and *B*, right) that are not found frequently on the productive VB1-8 $V_H(D)J_H$ alleles (Fig. 2 *A* and *B*, left), due to their propensity to inactivate functional IgH chain expression (6). Deletion endpoints in V_H1-2*02 passengers correlated with sites of high SHM (Pearson's r = 0.71–0.73; Fig. 2 *C–F*). In accord with their relative intrinsic SHM levels, the CDR3 portion of V_H1-2*02+$CDR3_{VB1-8}$ was highly targeted for deletions (Fig. 2*E*), whereas the CDR3 portion of the V_H1-2*02+ $CDR3_{VRC-PG04}$ passenger was not (Fig. 2*F*). In this regard, we note that primary SHM hotspot position 314 in the AGCT sequence of the CDR3 of V_H1-2*02+$CDR3_{VB1-8}$ passenger allele is slightly dampened in level compared with that of the identical $CDR3_{VB1-8}$ on the VB1-8 productive allele in the same experiments (Fig. S2*D*). This finding likely does not reflect dampened SHM levels per se but rather is caused by loss of B cells harboring AID-mediated V exon deletions on productive alleles due to impact of deletions on BCR expression and, thereby, B-cell viability (6).

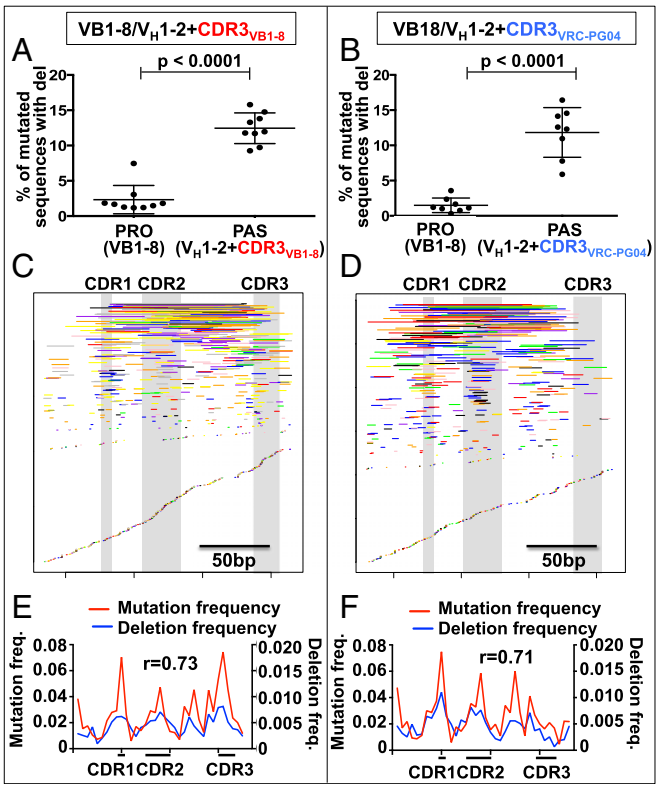

Fig. 2. Deletions in V_H1-2*02 passengers. (*A* and *B*) Deletion frequency, calculated as the percent of mutated sequences that contain deletions of (*A*) V_H1-2*02+$CDR3_{VB1-8}$ and (*B*) V_H1-2+$CDR3_{VRC-PG04}$ passenger alleles, ± SD (*C* and *D*) Map of unique deletions in (*C*) V_H1-2*02+$CDR3_{VB1-8}$ and (*D*) V_H1-2*02+ $CDR3_{VRC-PG04}$ passenger allele sequences. Deletions are represented by lines whose start and end indicate the start and end of the deletion. Deletions from each of the 9 V_H1-2*02+$CDR3_{VB1-8}$ and 8 V_H1-2*02+$CDR3_{VRC-PG04}$ chimeras are displayed with a different color. (*E* and *F*) The location of SHMs compared with the location of deletion endpoints. r is the Pearson correlation coefficient between SHM frequency and deletion endpoint frequency of each bin. n = 9 VB1-8/V_H1-2*02+$CDR3_{VB1-8}$ and 8 VB1-8/V_H1-2*02+$CDR3_{VRC-PG04}$ chimeras.

Etiology of Recurrently Mutated Nucleotides in VRC01-Class bnAbs. Comparison of the V_H1-2*02–encoded portions of six VRC01-class bnAb V(D)J exons revealed 10 positions, located in FWR1, CDR1, CDR2, and FWR3, that were "recurrently mutated" in each bnAb (Fig. 3 *A–C*). Recurrently mutated bnAb positions 56, 185, and 187 occurred at V_H1-2*02 positions with low intrinsic SHM frequency that were neither primary nor secondary intrinsic SHM hotspots (Fig. 3*C*, yellow bars). Notably, a set of V_H1-2*02 "silent" positions (at which SHMs do not change encoded amino acids) of intrinsic SHM frequency comparable to these three recurrently mutated positions were, on average, mutated in only one or two of the six VRC01-class bnAbs (Fig. 3 *D* and *E*). Based on the number of bnAbs mutated in each set of comparable silent positions, considered as a binomial distribution, we estimated the probability of SHMs occurring at positions 56, 185, and 187 in all six bnAb sequences to be low (P values ≤0.0019; Fig. 3*E*). Indeed this probability was significant when considered in the context of the rigorous Bonferroni-adjusted significance level (Fig. 3*E*). Therefore, SHMs are likely enriched among VRC01-class bnAbs at these three sites by positive selection. Positions 172 and 156 (Fig. 3*C*, white bars) also are not primary or secondary intrinsic hotspots but could not

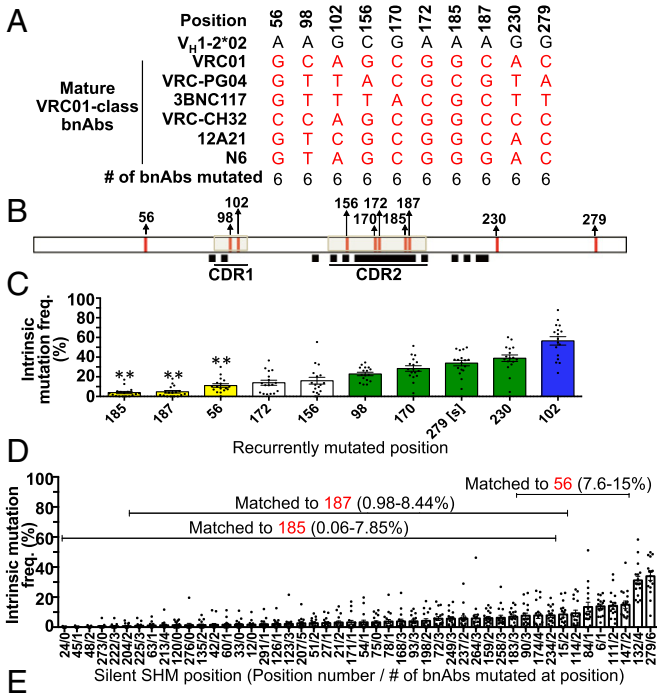

E

Pos	# of matched silent SHM positions mutated in following # of bnAbs:							p
	0	1	2	3	4	5	6	
185	7	9	10	11	2	1	0	0.0009 **
187	5	8	9	10	2	1	0	0.0013 **
56	0	2	5	1	1	0	0	0.0019 **

Fig. 3. Recurrently mutated V_H1-2*02 nucleotides among VRC01-class bnAbs. (*A*) Recurrently mutated V_H1-2*02 positions among the IgH V region exon sequences of potent VRC01-class bnAbs VRC01 (14), VRC-PG04 (14), 3BNC117 (14), VRC-CH32 (21, 26), 12A21 (14), and N6 (31). (*B*) Locations within the V_H1-2*02 sequence of recurrently mutated bnAb positions (red vertical lines) and of sequences that contribute to VRC01–gp120 contact sites [black squares (16)]. (*C*) Intrinsic mutation frequency of recurrently mutated bnAb positions calculated from V_H1-2*02 passenger sequences of mutational stratum 21–30 mutations per sequence. Data shown as mean ± SEM of nine VB1-8/V_H1-2*02+$CDR3_{VB1-8}$ and eight VB1-8/V_H1-2*02+$CDR3_{VRC-PG04}$ chimeras. [s] indicates that position 279 is a silent SHM position. Blue and green bars indicate primary and secondary hotspots. Yellow bars indicate positions for which there are silent SHM positions of V_H1-2*02 of comparable intrinsic mutation frequency. (*D*) Silent SHM positions of V_H1-2*02. *y* axis indicates intrinsic mutation frequency, calculated as in *C*. Brackets indicate the set of silent SHM positions that are matched in intrinsic mutation frequency to each of positions 185, 187, and 56. (*E*) The number of VRC01-class bnAb sequences mutated at silent SHM positions matched in intrinsic mutation frequency to positions 185, 187, and 56. p is the probability of matched silent SHMs being mutated in six of six bnAbs, estimated by modeling the number of silent SHM positions mutated in each number of bnAbs as a binomial distribution. In *C* and *E* ** indicates positions with *P* values < Bonferroni-adjusted α of 0.05/3.

be statistically analyzed due to insufficient numbers of matched silent positions. In this regard, silent SHM V_H1-2*02 positions have significantly lower intrinsic SHM frequencies than nonsilent SHM positions (Fig. S4*F*), possibly reflecting optimization of the V exon to target SHMs that change encoded amino acids. Five recurrently mutated VRC01-class bnAb positions occur in primary (position 102) or secondary (positions 230, 279, 170, and 98) V_H1-2*02 intrinsic SHM hotspots (Fig. 3*C*, blue and green bars), making them candidates for being recurrently mutated mainly due to high intrinsic SHM levels. Accordingly, recurrent position 279 is silent (Fig. 3*D*). We conclude that our approach discriminates between recurrent SHMs in VRC01-class bnAbs that occur at dominant intrinsic hotspots versus those that occur at low intrinsic SHM positions and are likely recurrent due to positive selection.

Influences of Affinity Maturation on Intrinsic SHM Targeting. To examine how SHM-targeting patterns on V_H1-2*02 exons change over the course of VRC01-class bnAb affinity maturation we assayed two VRC-PG04 bnAb lineage affinity maturation intermediates, termed int6.1% and int6.8% (21), as passengers and compared SHM patterns of their V_H1-2*02–encoded portion to that of V_H1-2*02. The int6.1% sequence diverges from V_H1-2*02 by 18 "prior" nucleotide changes and the int6.8% by 20 prior changes (Fig. 4*A*, red lines below int6.1% and int6.8% profiles and Fig. S5*A*). Comparison of the intrinsic SHM frequency at each site of prior SHMs between the two intermediate and the germline V_H1-2*02 revealed that the int6.1% and int6.8% sequences, respectively, had eight and five sites of prior SHMs that resulted in a significant difference in their intrinsic SHM frequency (Fig. 4*A*, asterisks). However, within sequence regions conserved between the intermediates and the germline V_H1-2*02 sequence, SHM targeting patterns were highly similar (Fig. 4*A*). For example, the SHM frequency of a region of CDR1 and FWR2 nucleotides adjacent to a robustly targeted AGCA hotspot in the CDR2 of int6.1% were not significantly altered between int6.1% and V_H1-2*02 (Pearson's $r = 0.98$) (Fig. S5*B*).

All five prior SHMs of the V_H1-2*02 portion of int6.8% that changed SHM targeting of a particular V_H1-2*02 position resulted in decreases in intrinsic SHM frequency due to inactivation of SHM motifs (Fig. 4*A*, downward arrows). For int6.1%, five of eight prior SHMs that changed SHM-targeting frequency were associated with decreased intrinsic SHM frequency due to SHM motif inactivation (Fig. 4*A*, downward arrows), but three were associated with increases (Fig. 4*A*, upward arrows). The latter three int6.1% positions included position 83, where a C-to-G SHM in FWR1 converted ACCT to the AGCT AID targeting motif (4.2-fold increase); position 161, where an A-to-G SHM in CDR2 converted AACA to the AGCA AID targeting motif (17-fold increase); and position 166, where a G-to-A SHM in CDR2 converted TGG in V_H1-2*02 to TAA but did not create an AID targeting motif (sevenfold increase) (Fig. S5*C*). We speculate that increased intrinsic SHM of position 166 most likely resulted via spreading from adjacent AID-targeted SHM hotspots to the newly generated polymerase eta TAA targeting motif (24). Notably, SHMs at positions 161 and 166 would produce amino acid changes at the VRC–PG04–gp120 interface (21). Thus, certain SHMs in a VRC-PG04-lineage intermediate promote further SHMs that may directly affect affinity maturation.

To assay how extensive affinity maturation influences the intrinsic SHM frequency of the V exon sequence we assayed the mature VRC-PG04 variable region sequence as a passenger and found that, compared with the V_H1-2*02 passenger, it had substantially reduced intrinsic SHM frequency relative to the productive VB1-8 control allele (Fig. 4*B* and Fig. S5*D*). Accordingly, of the seven V_H1-2*02 primary SHM hotspots (Fig. 1*B*) four were mutated in the final mature VRC-PG04 sequence, including one (position 92) that was the site of a 3-bp insertion (Fig. S5*E*). Another one (position 103) was inactivated as a DGYW by prior SHM of an adjacent primary hotspot (Fig. S5*E*). Notably, the G and the C at positions 9 and 10 within the FWR1 AGCT primary hotspot were not mutated and remained as SHM hotspots in the mature VRC-PG04 sequence (Fig. S5*E*), potentially reflecting negative selection against clones containing SHMs at these particular FWR sites. In addition, 21 of the 31 secondary hotspots identified in the 11–20 mutations per sequence stratum (Fig. 1*C*) were mutated in the VRC-PG04 sequence, including two (positions 181 and 182) that were the sites of another 3-bp insertion (Fig. S5*E*). Of the 10 secondary hotspot nucleotides that were not mutated in VRC-PG04, 9 were likely inactivated as hotspots via prior mutation of adjacent nucleotides that were in most cases themselves either primary or secondary hotspots (Table S1). Thus, the low intrinsic mutability of the mature VRC-PG04 variable region sequence derives, at least in substantial part, from SHM of primary or secondary SHM hotspots

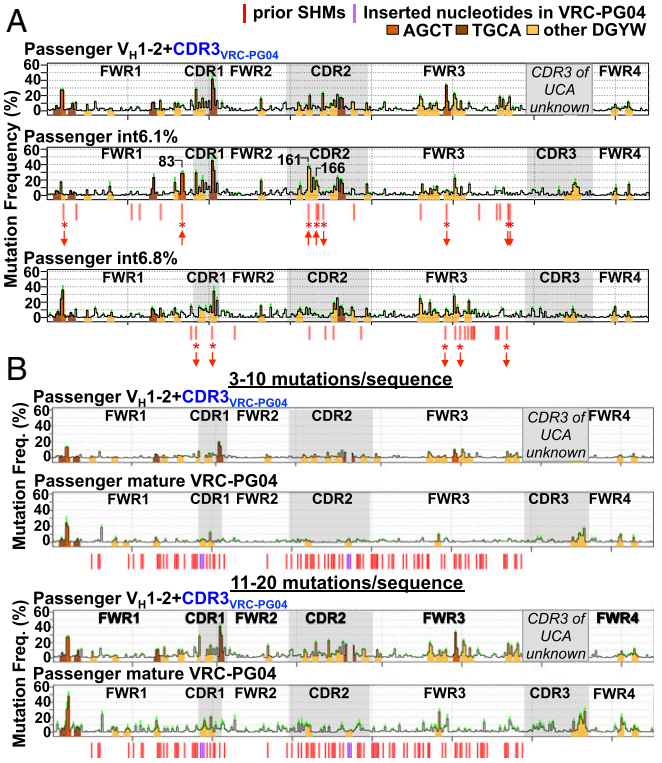

Fig. 4. SHM targeting of VRC-PG04 intermediates and mature VRC-PG04 passengers. (*A*) SHM profile of V$_H$1-2*02 and FWR4 portions of V$_H$1-2*02+CDR3$_{VRC-PG04}$ (*Top*, reproduced from Fig. 1*C*), int6.1% (*Middle*), and int6.8% passengers (*Bottom*). Data from intermediate mutational stratum 11–20 mutations per sequence is shown. *t* tests were performed comparing mean SHM frequency between germline V$_H$1-2*02 and int6.1% at the position of each of 18 prior SHMs, and comparing mean SHM frequency between V$_H$1-2*02 and int6.8% at the position of each of 20 prior SHMs. Significant differences of $P <$ Bonferroni-adjusted α of 0.05/18 for int6.1% or $P < 0.05/20$ for int6.8% are indicated by asterisks, and upward or downward arrows indicate whether SHM frequency of the intermediate was increased or decreased compared with V$_H$1-2*02 at the position. $n = 8$ V$_H$1-2*02+CDR3$_{VRC-PG04}$, 6 int6.1%, and 5 int6.8% chimeras, 3,000–5,000 mutated sequences per chimera. (*B*) SHM profiles of V$_H$1-2*02+CDR3$_{VRC-PG04}$ (reproduced from Fig. 1 *B* and *C*) and mature VRC-PG04 passenger allele sequences at 3–10 (*Top*) and 11–20 (*Bottom*) mutations per sequence. There were few (<100) mature VRC-PG04 passenger sequences with 21–30 mutations per sequence, and thus the SHM profile of this mutational level is not shown. $n = 8$ V$_H$1-2*02+CDR3$_{VRC-PG04}$ chimeras and 6 mature VRC-PG04 chimeras, 3,000–5,000 mutated sequences per chimera. In *A* and *B* red lines indicate positions of prior SHMs within V$_H$1-2*02 segment. CDR3 of unmutated common ancestor is not known for VRC-PG04 and therefore SHMs are not indicated for this region. Purple lines indicate the positions of two 3-bp insertions in CDR1 and CDR2. Productive allele mutation frequencies for these passengers are shown in Fig. S5*D*.

in the progenitor V(D)J exon into non-DGYW motifs over the course of affinity maturation.

Discussion

Our studies show that local sequence context is a more dominant determinant of VRC01-class bnAb intrinsic mutation frequency than long-range influences of hotspots at other sites within a VDJ exon. Introducing SHM hotspots into a V exon caused a global increase in overall V exon SHM frequency in cell-line studies (10, 11). However, we show that in vivo association of V$_H$1-2*02 with CDR3s that have high or low SHM potential did not markedly influence PP GC B-cell SHM frequency of V$_H$1-2*02 sequences, including that of adjacent FWR3 sequences or that of the most CDR3-proximal primary hotspot position. The only increase in SHM frequency observed was at position 293, which is 2 bp upstream of the CDR3 and thus could have been influenced by adjacent sequence differences created by the V$_H$-to-DJ$_H$ junction. Our findings also contrast with those of transgene studies that indicated that introduced hotspots lead to compensatory decreases in SHM frequency elsewhere in the V(D)J exon (9), because we did not observe a change in V$_H$1-2*02 SHM frequency in passengers containing CDR3s with high or low SHM potential. Likewise, we also found that SHM patterns of V$_H$1-2*02 in association with diverse CDR3s of V(D)J exons assembled in vivo were highly similar to that of the V$_H$1-2*02 passenger exons with fixed CDRs that had high or low SHM potential. Together, our studies suggest that neither introduction of new SHM hotspots nor saturation of existing SHM hotspots has a major general influence on SHM across V(D)J exons in GC B cells.

Certain SHMs in V$_H$1-2*02–using antibodies may be intrinsically favored (15, 25). Our findings indeed demonstrate that a number of recurrently mutated VRC01-class bnAb positions occur at primary or secondary V$_H$1-2*02 SHM hotspots. Of these, only one (position 170) encodes an amino acid at the VRC01–gp120 interface (16), and another (position 270) is silent, supporting the notion that most of these recurrent SHMs may occur due to high intrinsic SHM frequency in the absence of positive or negative selection. We also identified three recurrently mutated V$_H$1-2*02 positions with quite low intrinsic SHM frequencies that, based on strict statistical analyses, are not predicted to occur recurrently. Thus, these SHMs are likely enriched by positive selection, a notion supported by two such positions (185 and 187) affecting the VRC01–gp120 interface (Fig. 3*B*). Our findings that V exon deletions also correlate with sites of high intrinsic SHM (6) (Fig. 2) suggest that intrinsic SHM frequency data should be applicable for assessing impact of intrinsic SHM frequency on deletions (or insertions) in VRC01-class bnAbs (26). By extending our matched silent SHM position-based analysis to positions mutated in five out of six bnAbs, we identified eight additional, nonsilent positions with intrinsic SHM frequencies (Fig. S4*C*) that had a relatively low probability of occurring without selection ($P \leq 0.0341$; Fig. S4 *C* and *E*). However, none of these reached Bonferroni-adjusted significance (Fig. S4*E*). If additional VRC01-class bnAbs are identified and added to the six currently available, it may be possible to better clarify whether or not any of these eight potential additional positions become stronger candidates for positive selection. Overall, the methods we describe to identify recurrent bnAb SHMs (and deletions) that depend on strong positive selection, along with our recent mouse models (22), could contribute to studies aimed at designing immunogens to accelerate development of bnAb lineages (27).

Our finding that local sequence context affects intrinsic SHM frequency implies that different VDJ exon sequences, including intermediates along a particular lineage, will have different local potentials for affinity maturation. In this regard, the two VRC01-lineage affinity maturation intermediates that we assayed had different potentials to promote particular SHMs that would affect the bnAb–gp120 interface (Fig. 4*A*). Such findings again may be relevant to the design of sequential immunization strategies to drive B cells along desired bnAb maturation pathways (12, 28, 29), because leading a response through one intermediate versus another may influence the frequency with which particular SHMs are generated. However, overall intrinsic SHM levels of a highly mutated mature VRC-PG04 bnAb are very low due to loss of intrinsic SHM targets due to high intrinsic SHM hotspot mutability and/or by selection for SHMs that inactivate them (Fig. 4*B*). To further increase potency and breadth of such bnAbs for therapeutic goals, increased SHM potential might be gained by embedding AID targeting motifs into the mature bnAb V exon sequence, while preserving key interaction residues. Another approach might be to modify a germline bnAb precursor to contain the intrinsically low SHMs that are functionally implicated by recurrent presence in bnAbs lineages. These and related approaches again could be facilitated by our rapidly generated and more physiological V(D)J-rearranging

vaccination mouse models that are designed to test HIV-1 immunization strategies (22).

Materials and Methods

Generation of Targeted ES Cells and Mouse Chimeras. ES cell lines containing passenger alleles were generated as previously described (6). Briefly, an ES cell line containing a VB1-8 productive allele and a puromycin cassette in place of the V(D)J exon on the other allele was generated. ES cell lines containing passenger alleles were generated by replacing the puromycin cassette with the respective passenger test sequences. Finally, the modified ES cells were used to generate chimeric mice with totally ES-cell-derived B and T lymphocytes via our RAG-2 blastocyst complementation (19). See *SI Materials and Methods* for details.

GC B-Cell Isolation. PP were collected from 8- to 12-wk-old passenger allele chimeras or V_H1-2*02–rearranging mice (22) that were immunized with NP-CGG (N-5055E; Biosearch Technologies) for 10 d. This short-term immunization does not influence SHM patterns of either productive or passenger VB1-8 alleles in splenic or PP GC B cells (6). However, due to their higher level SHM levels, which occur even without immunization (6), we focused our analyses on PP GC B cells, which were isolated by flow cytometric sorting of $B220^+$/Peanut $Agglutinin^{hi}$ B cells.

PCR and Sequencing. Productive and passenger alleles were amplified in separate PCR reactions using allele-specific primers (see Table S2 for primer sequences and *SI Materials and Methods* for PCR conditions). The products were sequenced by Illumina MiSeq high-throughput sequencing (Illumina).

Sequencing Alignment and Analysis for Productive and Passenger Alleles. Miseq sequencing data reads were demultiplexed using the fastq-multx tool from ea-utils (https://expressionanalysis.github.io/ea-utils/) and Illumina adaptor sequences trimmed using the SeqPrep utility (https://github.com/jstjohn/SeqPrep) and aligned to a reference sequence using Bowtie2 (30). A custom script was used to call mutations. A nucleotide differing from the reference sequence was counted as a mutation only if the Illumina Sequencing Quality Score was >20, corresponding to a probability of <0.01 that the base was called incorrectly. A custom pipeline was used to process the sequencing data and to call mutations. SHM frequencies are calculated as the percent of sequences containing a mutation at the indicated nucleotide(s). Duplicate sequences are retained. As described previously (6), we control for PCR repeats by analyzing at least five independent mouse replicates for each experiment and then averaging mutation frequency of a given nucleotide across replicates.

Detection of Differences Between SHM Profiles at Individual Nucleotides. To detect whether the intrinsic SHM pattern of V_H1-2*02+$CDR3_{VB1\text{-}8}$ and V_H1-2*02+$CDR3_{VRC\text{-}PG04}$ differs significantly at any individual nucleotide we performed an unpaired *t* test comparing the mutation frequency of the two passengers at each of the 294 nucleotide positions of the V_H1-2*02, at each mutational stratum. To correct for multiplicity of testing we applied a Bonferroni-adjusted *P* value cutoff for significance of 0.05/294. The SHM profile of the V_H1-2*02–rearranging mice was compared with each of the V_H1-2*02 passengers by the same method.

Detection of Positively Selected SHMs in VRC01-Class bnAbs. We selected VRC01-class bnAb sequences with high breadth and potency for analysis, using the criteria that they neutralized >75% of tested HIV isolates with an IC_{50} <50 μg/mL. In addition, each bnAb analyzed came from a different donor, ensuring that all SHMs in a given bnAb assayed occurred independently of those in other assayed bnAbs. To determine a set of silent mutation positions of V_H1-2*02 matched in intrinsic mutation frequency to each recurrently mutated bnAb position, for each recurrently mutated position we tested the significance of the difference of its mean intrinsic mutation frequency with that of each silent SHM position of V_H1-2*02 (shown in Fig. 3*D* and Fig. S4*D*) by ANOVA with Fisher's least significant difference post hoc test. A silent mutation position was considered to be of mutation frequency similar to that of the recurrently mutated position if $P > 0.05$. Nominal probabilities of matched silent SHM positions being mutated in each number of bnAbs were estimated by modeling the frequency distribution of silent SHM positions mutated in each number of bnAbs as a binomial distribution.

ACKNOWLEDGMENTS. We thank Pei-Yi Huang and Yuko Fujiwara for generating the chimeras and Kenneth Ketman and Natasha Barteneva for help with FACS sorting. This work was supported by NIH Grants R01AI077595 and CHAVI-ID 5UM1AI100645 (to F.W.A); the Intramural Research Program of the Vaccine Research Center, National Institute of Allergy and Infectious Diseases, NIH; NIH Grant F30AI114179- 01A1 (to J.K.H.); NIH Grant 1U19AI117892-02 (to T.B.K.); and Dana Farber/Harvard Cancer Center Core Grant 5P30 CA006516 (to D.N.). F.W.A. is an investigator and Z.D. is a postdoctoral fellow of the Howard Hughes Medical Institute. L.-S.Y. was a Cancer Research Institute postdoctoral fellow.

1. Alt FW, Zhang Y, Meng FL, Guo C, Schwer B (2013) Mechanisms of programmed DNA lesions and genomic instability in the immune system. *Cell* 152:417–429.
2. Amzel LM, Poljak RJ (1979) Three-dimensional structure of immunoglobulins. *Annu Rev Biochem* 48:961–997.
3. Mostoslavsky R, Alt FW, Rajewsky K (2004) The lingering enigma of the allelic exclusion mechanism. *Cell* 118:539–544.
4. Victora GD, Nussenzweig MC (2012) Germinal centers. *Annu Rev Immunol* 30:429–457.
5. Hwang JK, Alt FW, Yeap LS (2015) Related mechanisms of antibody somatic hypermutation and class switch recombination. *Microbiol Spectr* 3:MDNA3-0037-2014.
6. Yeap LS, et al. (2015) Sequence-intrinsic mechanisms that target AID mutational outcomes on antibody genes. *Cell* 163:1124–1137.
7. Rogozin IB, Diaz M (2004) Cutting edge: DGYW/WRCH is a better predictor of mutability at G:C bases in Ig hypermutation than the widely accepted RGYW/WRCY motif and probably reflects a two-step activation-induced cytidine deaminase-triggered process. *J Immunol* 172:3382–3384.
8. Dörner T, et al. (1997) Analysis of the frequency and pattern of somatic mutations within nonproductively rearranged human variable heavy chain genes. *J Immunol* 158:2779–2789.
9. Goyenechea B, Milstein C (1996) Modifying the sequence of an immunoglobulin V-gene alters the resulting pattern of hypermutation. *Proc Natl Acad Sci USA* 93:13979–13984.
10. Baughn LB, et al. (2011) Recombinase-mediated cassette exchange as a novel method to study somatic hypermutation in Ramos cells. *MBio* 2:e00186-11.
11. Wei L, et al. (2015) Overlapping hotspots in CDRs are critical sites for V region diversification. *Proc Natl Acad Sci USA* 112:E728–E737.
12. Mascola JR, Haynes BF (2013) HIV-1 neutralizing antibodies: Understanding nature's pathways. *Immunol Rev* 254:225–244.
13. Kwong PD, Mascola JR (2012) Human antibodies that neutralize HIV-1: Identification, structures, and B cell ontogenies. *Immunity* 37:412–425.
14. Scheid JF, et al. (2011) Sequence and structural convergence of broad and potent HIV antibodies that mimic CD4 binding. *Science* 333:1633–1637.
15. Bonsignori M, et al.; NISC Comparative Sequencing Program (2016) Maturation pathway from germline to broad HIV-1 neutralizer of a CD4-mimic antibody. *Cell* 165:449–463.
16. Zhou T, et al. (2010) Structural basis for broad and potent neutralization of HIV-1 by antibody VRC01. *Science* 329:811–817.
17. Burton DR, Mascola JR (2015) Antibody responses to envelope glycoproteins in HIV-1 infection. *Nat Immunol* 16:571–576.
18. Jardine JG, et al. (2016) Minimally mutated HIV-1 broadly neutralizing antibodies to guide reductionist vaccine design. *PLoS Pathog* 12:e1005815.
19. Chen J, Lansford R, Stewart V, Young F, Alt FW (1993) RAG-2-deficient blastocyst complementation: An assay of gene function in lymphocyte development. *Proc Natl Acad Sci USA* 90:4528–4532.
20. Cumano A, Rajewsky K (1985) Structure of primary anti-(4-hydroxy-3-nitrophenyl)acetyl (NP) antibodies in normal and idiotypically suppressed C57BL/6 mice. *Eur J Immunol* 15:512–520.
21. Wu X, et al.; NISC Comparative Sequencing Program (2011) Focused evolution of HIV-1 neutralizing antibodies revealed by structures and deep sequencing. *Science* 333:1593–1602.
22. Tian M, et al. (2016) Induction of HIV neutralizing antibody lineages in mice with diverse precursor repertoires. *Cell* 166:1471–1484 e1418.
23. Rada C, Yélamos J, Dean W, Milstein C (1997) The 5′ hypermutation boundary of kappa chains is independent of local and neighbouring sequences and related to the distance from the initiation of transcription. *Eur J Immunol* 27:3115–3120.
24. Rogozin IB, Pavlov YI, Bebenek K, Matsuda T, Kunkel TA (2001) Somatic mutation hotspots correlate with DNA polymerase eta error spectrum. *Nat Immunol* 2:530–536.
25. Sheng Z, et al.; NISC Comparative Sequencing Program (2017) Gene-specific substitution profiles describe the types and frequencies of amino acid changes during antibody somatic hypermutation. *Front Immunol* 8:537.
26. Kepler TB, et al. (2014) Immunoglobulin gene insertions and deletions in the affinity maturation of HIV-1 broadly reactive neutralizing antibodies. *Cell Host Microbe* 16:304–313.
27. Bonsignori M, et al. (2017) Antibody-virus co-evolution in HIV infection: Paths for HIV vaccine development. *Immunol Rev* 275:145–160.
28. Haynes BF, Kelsoe G, Harrison SC, Kepler TB (2012) B-cell-lineage immunogen design in vaccine development with HIV-1 as a case study. *Nat Biotechnol* 30:423–433.
29. Escolano A, et al. (2016) Sequential immunization elicits broadly neutralizing anti-HIV-1 antibodies in Ig knockin mice. *Cell* 166:1445–1458 e1412.
30. Langmead B, Salzberg SL (2012) Fast gapped-read alignment with Bowtie 2. *Nat Methods* 9:357–359.
31. Huang J, et al. (2016) Identification of a CD4-binding-site antibody to HIV that evolved near-pan neutralization breadth. *Immunity* 45:1108–1121.
32. Sonoda E, et al. (1997) B cell development under the condition of allelic inclusion. *Immunity* 6:225–233.
33. Han L, Masani S, Yu K (2011) Overlapping activation-induced cytidine deaminase hotspot motifs in Ig class-switch recombination. *Proc Natl Acad Sci USA* 108:11584–11589.
34. Lin SG, et al. (2016) Highly sensitive and unbiased approach for elucidating antibody repertoires. *Proc Natl Acad Sci USA* 113:7846–7851.
35. Pham P, Bransteitter R, Petruska J, Goodman MF (2003) Processive AID-catalysed cytosine deamination on single-stranded DNA simulates somatic hypermutation. *Nature* 424:103–107.